AMERICAN SOCIETY FOR MICROBIOLOGY | Molecular and Cellular Biology

Inositol Pyrophosphate Kinase Asp1 Modulates Chromosome Segregation Fidelity and Spindle Function in *Schizosaccharomyces pombe*

Boris Topolski, Visnja Jakopec, Natascha A. Künzel, Ursula Fleig

Institut für Funktionelle Genomforschung der Mikroorganismen, Eukaryotische Mikrobiologie, Heinrich-Heine-Universität, Düsseldorf, Germany

Chromosome transmission fidelity during mitosis is of critical importance for the fitness of an organism, as mistakes will lead to aneuploidy, which has a causative role in numerous severe diseases. Proper segregation of chromosomes depends on interdependent processes at the microtubule-kinetochore interface and the spindle assembly checkpoint. Here we report the discovery of a new element essential for chromosome transmission fidelity that implicates inositol pyrophosphates (IPPs) as playing a key role in this process. The protein is Asp1, the *Schizosaccharomyces pombe* member of the highly conserved Vip1 family. Vip1 enzymes are bifunctional: they consist of an IPP-generating kinase domain and a pyrophosphatase domain that uses such IPPs as substrates. We show that Asp1 kinase function is required for bipolar spindle formation. The absence of Asp1-generated IPPs resulted in errors in sister chromatid biorientation, a prolonged checkpoint-controlled delay of anaphase onset, and chromosome missegregation. Remarkably, expression of Asp1 variants that generated higher-than-wild-type levels of IPPs led to a faster-than-wild-type entry into anaphase A without an increase in chromosome missegregation. In fact, the chromosome transmission fidelity of a nonessential chromosome was enhanced with increased cellular IPPs. Thus, we identified an element that optimized the wild-type chromosome transmission process.

In eukaryotes, the faithful transmission of genetic information from one generation to the next is tightly controlled. Genome instability generally has a strong negative impact on the fitness of an organism. Decreased chromosome segregation fidelity during cell division will give rise to cell progeny which have lost or gained chromosomes. Aneuploidy is a distinguishing feature of many types of cancer and neurological diseases and has been implicated as an important factor in the aging process (1, 2). It is a poorly understood paradox that genome plasticity can also be advantageous for the propagation of cells or an organism. Aneuploid tumor cells have a proliferative advantage, and large-scale chromosome changes are a common feature of human-pathogenic fungi such as *Candida*. In the latter case, these alterations facilitate an adaption to the environment resulting in increased survival (3).

Chromosome segregation is a precise process: in model yeasts such as the fission yeast *Schizosaccharomyces pombe* where *in vivo* chromosome loss rates can be determined easily, it is approximately 0.01% (reviewed in reference 4). Chromosome transmission fidelity depends on the formation and function of the bipolar spindle, the multicomponent kinetochore complex assembled on centromeric chromatin, and the correct connections between these two structures. Biorientation of sister chromatids requires the binding of plus ends of spindle microtubules (MTs) to attachment sites on the kinetochore in such a way that sisters are bound to MTs polymerized from opposing spindle poles. Incorrect attachments are common and are corrected by the Aurora B kinase family, whose phosphorylation of specific kinetochore proteins weakens incorrect MT-kinetochore binding (reviewed in reference 5). The process of MT-kinetochore attachment is monitored by the spindle assembly checkpoint (SAC) (reviewed in reference 6), which also seems to play an active role in achieving chromosome biorientation (7).

Spindle assembly in *S. pombe* is similar to that in other eukaryotes and can be divided into three phases corresponding to prometaphase (I), metaphase/anaphase A (II), and anaphase B (III). Phase I spindles rapidly elongate to approximately 1.5 μm, while phase II spindles are much less dynamic, with a length of up to 3 μm. Phase III spindles rapidly elongate to 10 to 12 μm (8, 9). In phase II, sister chromosomes need to become bioriented, and the cell will stay in this phase until biorientation has been achieved.

In this work, we describe a new modulator of all 3 spindle phases: inositol pyrophosphates (IPPs) generated by the Asp1 kinase. Asp1 is a member of the highly conserved Vip1 protein family. Vip1 proteins have a dual-domain structure that consists of an N-terminal "RimK"/ATP-grasp superfamily kinase domain and a C-terminal domain with homology to histidine-acid phosphatases (10–13). Both domains are enzymatically active. The function of the N-terminal kinase domain has been studied extensively, and it has been demonstrated that the enzymatic activity is highly specific: generation of diphospho-*myo*-inositol polyphosphates (here called inositol pyrophosphates [IPPs]) by adding a phosphate at position 1 on the fully phosphorylated inositol ring (11, 12, 14, 15). We showed recently that *in vitro* the C-terminal Asp1 domain

Received 8 June 2016 **Returned for modification** 7 July 2016
Accepted 29 September 2016

Accepted manuscript posted online 3 October 2016

Citation Topolski B, Jakopec V, Künzel NA, Fleig U. 2016. Inositol pyrophosphate kinase Asp1 modulates chromosome segregation fidelity and spindle function in *Schizosaccharomyces pombe*. Mol Cell Biol 36:3128–3140. doi:10.1128/MCB.00330-16.

Address correspondence to Ursula Fleig, fleigu@hhu.de.

B.T., V.J., and N.A.K. contributed equally to this article.

Supplemental material for this article may be found at http://dx.doi.org/10.1128/MCB.00330-16.

TABLE 1 *S. pombe* strains used in this study

Strain	Genotype	Source (alternative strain name)
UFY2156	*h*$^-$ SV40::GFP-Atb2$^+$::*LEU2 his3-D1*	Yeast Genetic Resource Center, Osaka, Japan
UFY1511	*h*$^+$ *asp1*^{D333A}::Kan^r *his3-D1 ade6-M210 leu1-32 ura4-D18*	U. Fleig
UFY1579	*h*$^+$ *asp1*^{H397A}::Kan^r *his3-D1 ade6-M210 leu1-32 ura4-D18*	U. Fleig
UFY2279	*h*$^-$ *asp1*^{H397A}::Kan^r SV40::GFP-Atb2$^+$::*LEU2*	This study
UFY2280	*h*$^-$ *asp1*^{D333A}::Kan^r SV40::GFP-Atb2$^+$::*LEU2 his3-D1*	This study
UFY605	*h*$^-$ *his3-D1 ade6-M210 leu1-32 ura4-D18*	K. Gould (425)
UFY857	*h*$^-$ Kan^r::*nmt81*::GFP-Atb2$^+$ *leu1-32*	T. Toda
UFY1763	*h*$^+$ *asp1*^{H397A}::Kan^r Kan^r::*nmt81*::GFP-Atb2$^+$ *leu1-32 ura4-D18*	U. Fleig
UFY1529	*h*$^+$ *asp1*^{D333A}::Kan^r Kan^r::*nmt81*::GFP-Atb2$^+$ *leu1-32 ura4-D18*	U. Fleig
UFY2249	*h*$^-$ Sad1-mCherry::Kan^r LacI-GFP::*his7*$^+$ LacO-repeat::*lys1*$^+$ *ura4-D18 leu1-32*	This study
UFY2242	*h*$^-$ *asp1*^{D333A}::Kan^r Sad1-mCherry::Kan^r LacI-GFP::*his7*$^+$ LacO-repeat::*lys1*$^+$	This study
UFY2357	*h*$^+$ *ark1*$^+$-GFP::Kan^r *sid4*$^+$-mCherry::Nat^r	Silke Hauf (SK402)
UFY2363	*h*$^-$ *ark1*$^+$-GFP::Kan^r Sid4$^+$-mCherry::Nat^r *asp1*^{D333A}::Kan^r	This study
UFY1543	*h*$^+$ *asp1*^{D333A}::Kan^r *mph1*Δ::*ura4*$^+$ *his3-D1 ade6-M216 leu1-32 ura4-D18*	This study
UFY2337	*h*$^-$ *asp1*^{D333A}::Kan^r *mph1*Δ::*ura4*$^+$ SV40::GFP-Atb2$^+$::*LEU2 ura4-D18*	This study
UFY2367	*h*$^-$ *asp1*^{H397A}::Kan^r Sad1-mCherry::Kan^r LacI-GFP::*his7*$^+$, LacO-repeat::*lys1*$^+$ *ura4-D18 leu1-32*	This study
UFY2646	*h*$^-$ *asp1*^{D333A}::Kan^r *mph1*Δ::*ura4*$^+$ LacI-GFP::*his7*$^+$ LacO-repeat::*lys1*$^+$ Sad1-mCherry::Kan^r *his*$^-$ *lys1-131 ura4-D18 leu1-32*	This study
UFY2627	*h*$^-$ *mph1*Δ::*ura4*$^+$ LacI-GFP::*his7*$^+$ LacO-repeat::*lys1*$^+$ Sad1-mCherry::Kan^r *leu1-32 ura4-D18 his*$^-$ *lys1-131*	This study
UFY138	*h*$^-$ *mph1*Δ::*ura4*$^+$ *leu1-32 ura4-D18 ade6-M216*	Shalley Sazer
UFY103	*h*$^-$ *ade6-M210 leu1-32 ura4-D6* Ch16[*ade6-M216*]	Mitsuhiro Yanagida (10.2.2)
UFY2336	*leu1-32*::SV40::Atb2$^+$-GFP[*LEU2*] *mad2*Δ::*ura4*$^+$ *ura4-D18*	This study
UFY2335	*leu1-32*::SV40::Atb2$^+$-GFP[*LEU2*] *asp1*^{D333A}::Kan^r *mad2*Δ::*ura4*$^+$ *ura4-D18*	This study
UFY1790	*h*$^-$ *asp1*^{D333A}::Kan^r *ade6-M210 leu1-32*	This study
UFY139	*h*$^-$ *mad2*Δ::*ura4*$^+$ *leu1-32 ura4-D18 ade6-M210*	Shelley Sazer
UFY2215	*h*$^-$ *asp1*^{D333A}::Kan^r *mad2*Δ::*ura4*$^+$ *ura4-D18 leu1-32*	This study
UFY229	*h*$^-$ *cut7-466 leu1-32*	Iain Hagan (138)
UFY2422	*h*$^+$ *klp6*Δ::Kan^r *leu1 ura4 his2/7*	Takashi Toda (AR018)
UFY302	*h*$^-$ *pkl1*Δ::*his3*$^+$ *leu1-32 ura4-D18 ade6-210 his3-D1*	Robin Allshire and Alison Pidoux (ALP192)

reduces the IPP output of the kinase domain, indicating that it has phosphatase activity (16). Again, this enzymatic activity is highly substrate specific, as *in vitro* analysis showed that the C-terminal Asp1 domain hydrolyzes the diphosphate exclusively at position 1 of the inositol ring (17). Vip1 members regulate a wide variety of eukaryotic processes ranging from the human antiviral response to plant defense mechanisms against insects (10, 11, 18–20). In fission yeast, the Vip1 member Asp1 regulates the dimorphic switch, which is a dramatic morphological alteration in response to changing environmental conditions (21). How the Asp1 kinase controlled dimorphic switch functions at the molecular level is not fully understood. However, we have recently shown that fungal Vip1 family members regulate morphogenesis by modulating the interphase MT cytoskeleton (16).

Our present analysis now extends the number of cellular processes controlled by Vip1 kinases, as we find that mitotic fidelity is dependent on Asp1 kinase function.

MATERIALS AND METHODS

Strains and media. All *S. pombe* strains used are listed in Table 1. New strains were obtained by crossing the initial strains, followed by random spore analysis and phenotype determination. Strains were grown in full medium (YE5S) or minimal medium (MM) with supplements (22). For *nmt81*::*gfp-atb2*$^+$ expression, cells were grown in MM without thiamine for 24 h at 30°C before analysis.

For live-cell imaging, cells were preincubated overnight at 30°C or 25°C, diluted to 10^5 cells/ml, and grown for additional 24 h in MM. Microscopy slides were prepared by patching cells on agarose pads as described previously (23).

Microscopy. For live-cell imaging, a Zeiss spinning-disk confocal microscope equipped with an AxioCam MRm camera (photomicrographs in Fig. 2 and in Fig. S3 in the supplemental material) or a Rolera EM-C^2 (QImaging) camera (all other photomicrographs) and AxioVision and Zen2011/2012 software was used. Image processing was done with Adobe Photoshop CS2 (Adobe Systems Software Ireland Limited, Dublin, Ireland). A z-stack of 15 z slices with a distance of 0.5 μm was recorded and a maximum-intensity projection (MIP) created. The time interval between images was 10 to 30 s. For technical reasons, microscopic analysis was done at 20°C. For spindle midzone measurements, images were taken every 10 s. The MIP image of the spindle with the thinnest midzone was used for measurement. The signal intensity of green fluorescent protein (GFP) fluorescence in live-cell images was determined with ImageJ 1.44 (NIH).

Western blot analysis. To determine expression of the plasmid-borne variant encoding positions 1 to 364 of Asp1 fused to GFP (*asp1*$^{1–364}$*-gfp*) via the *nmt1*$^+$ promoter, transformants were grown in MM with or without thiamine for 24 h at 30°C before protein extraction. Preparation of protein extracts, determination of protein concentrations, and Western blot analysis were carried out as described previously (16) using anti-GFP antibody (monoclonal mouse; Roche) and anti-γ-tubulin antibody (monoclonal mouse; Sigma).

Ch16 chromosome loss assay. The Ch16-containing strain was pregrown on MM without adenine to select for the presence of the Ch16 chromosome in cells. Such cells were transformed with a control vector or a plasmid expressing *asp1*$^{1–364}$ via the thiamine-repressible *nmt1*$^+$ promoter. Transformants were grown under plasmid and Ch16 selective conditions in the absence or presence of 5 μg/ml thiamine for 20 h at 25°C. Up to 30,000 cells per transformant were plated on plasmid-selective plates with a limiting amount of adenine and with or without thiamine for 10

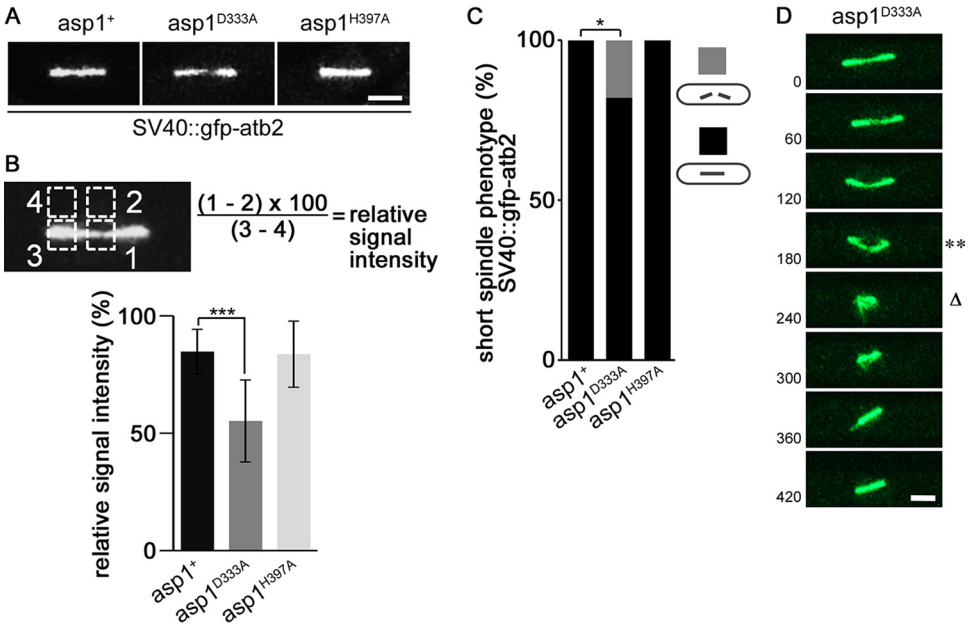

FIG 1 Asp1-generated IPPs control spindle midzone stability. (A) Photomicrographs of *asp1*$^{+}$, *asp1*^{D333A}, and *asp1*^{H397A} cells with a short (3- to 5-μm) spindle expressing SV40::GFP-Atb2^{+}. Bar, 2 μm. (B) Quantification of the fluorescence signal of the spindle midzone. The thinnest part of a spindle midzone was measured (square 1), and the fluorescent background was subtracted (square 2). For relative signal intensity this value was set in relation to the fluorescence signal of a spindle end (square 3) minus fluorescent background (square 4). Relative signal intensities of spindle midzones: *asp1*$^{+}$, 84.7 ± 9.5; *asp1*^{D333A}, 55.1 ± 17.5; and *asp1*^{H397A}, 83.6 ± 14.1 (n = 9/strain; ***, $P < 0.0005$ as determined by two-sample t test). (C) Quantification of spindle phenotypes (gray and black bars show broken and nonbroken spindles, respectively) determined for the indicated strains expressing SV40::GFP-Atb2^{+} (*asp1*$^{+}$ strain, n = 24; *asp1*^{H397A} strain, n = 22; *asp1*^{D333A} strain, n = 17; *, $P < 0.05$ as determined using χ^2 test). (D) Representative example of an *asp1*^{D333A} SV40::GFP-Atb2^{+} cell. Time between images, 60 s. Bar, 2 μm. **, collapsing spindle; Δ, broken spindle.

days at 25°C. Ch16 chromosome loss results in adenine prototrophy and red cells. Thus, chromosome loss in a growing colony was identified as red sectors within the white colony.

RESULTS

Asp1-generated IPPs are required for spindle assembly. To determine whether Asp1-generated IPPs had a role in spindle assembly, we looked at spindle structures using GFP–α-tubulin strains that expressed endogenously one of the three Asp1 variants Asp1, Asp1^{D333A}, or Asp1^{H397A} (21). Asp1 is encoded by the wild-type *asp1*$^{+}$ gene, while *asp1*^{D333A} generates an Asp1 variant that has a single amino acid change at position 333, which is the key catalytic residue for IPP kinase activity (10). Thus, Asp1^{D333A} cannot generate IPPs (10, 16). The Asp1^{H397A} variant has a mutation in a highly conserved histidine residue, which abolishes the C-terminal pyrophosphatase activity (16). Thus, the IPP output of Asp1^{H397A} is higher than that of the wild-type Asp1 protein (up to twice as much in an *in vitro* assay [16]). Therefore, the *asp1*^{D333A} strain cannot generate Asp1-made IPPs, the *asp1*$^{+}$ strain generates wild-type IPP amounts, and the *asp1*^{H397A} strain generates amounts of IPP that are increased compared to those of the wild-type strain.

The presence of GFP–α-tubulin (SV40::GFP-Atb2) (24) in the different *asp1* strains did not affect their growth on rich YE5S medium but slightly increased their sensitivity to the MT-destabilizing drug thiabendazole (TBZ) (see Fig. S1A in the supplemental material). Live-cell imaging of the spindles in the various mutant strains revealed that in contrast to *asp1*$^{+}$ spindles, *asp1*^{D333A} spindles were often aberrant, as they displayed an abnormally thin spindle midzone (Fig. 1A; Movies S1 and S2 in the supplemental material show an *asp1*$^{+}$ spindle and an *asp1*^{D333A} spindle, respectively). The spindle midzone consists of interpolar MTs coming from the two separated spindle pole bodies (SPBs). The plus ends of such MTs interdigitate via specific MT-associated proteins, thus giving stability to the spindle midzone (reviewed in reference 25). The *asp1*^{D333A} mutant spindles were between 3 and 5 μm in length, and the relative fluorescence signal intensity of the spindle midzone was significantly reduced compared to that of the midzones of *asp1*$^{+}$ spindles (84.7 ± 9.5 and 55.1 ± 17.5 for *asp1*$^{+}$ and *asp1*^{D333A}, respectively) (Fig. 1B). The thin spindle midzone phenotype was not observed in the *asp1*$^{+}$ and *asp1*^{H397A} strains (Fig. 1A and B). Interestingly, 18% of *asp1*^{D333A} mitotic cells showed spindle breakage (Fig. 1C). A typical example of such a phenotype in which the spindle collapsed and then reformed is shown in Fig. 1D.

Although expression of a GFP-tubulin construct is necessary for live-cell imaging of the MT cytoskeleton, it has been noted that expression of such constructs can affect MT behavior and dynamics (26). For example, it has been reported that strains expressing *nmt81*::GFP-Atb2 at the *atb2*$^{+}$ locus have altered MT properties (24, 27–29). The reason for this is unclear. However, it has been shown that the ratio of tagged GFP–α-tubulin to untagged α-tubulin is higher in the *nmt81*::GFP-Atb2 strain than in the SV40::GFP-Atb2 strain (26). We found that under our assay conditions, the presence of *nmt81*::GFP-Atb2 in the *asp1*$^{+}$ strain gave rise to short spindles that broke in 16% of cases (Fig. 2A and B, left panel). We therefore asked whether in the *nmt81*::GFP-Atb2 background the frequency of the *asp1*^{D333A} spindle phenotype was increased relative to that in wild-type cells. We found that short

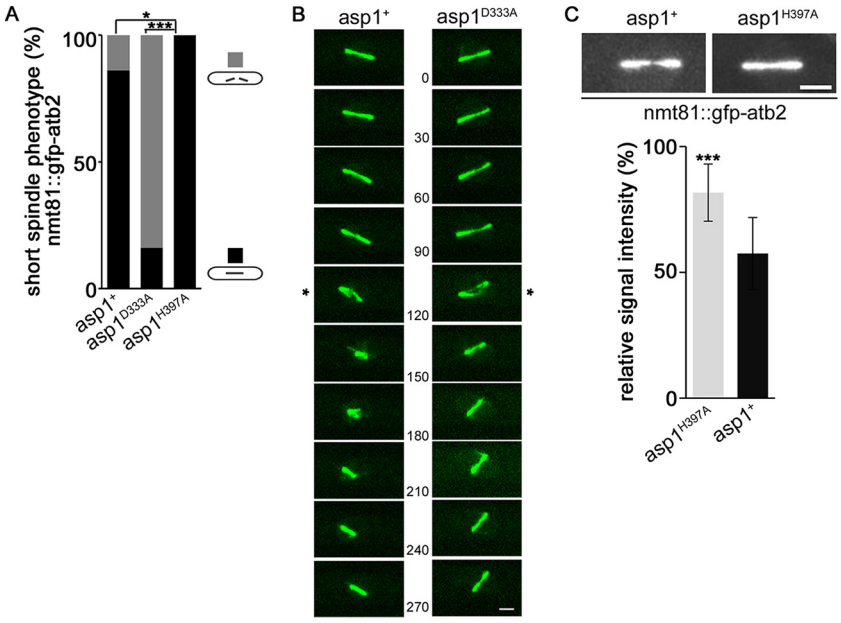

FIG 2 Aberrant spindle phenotype of an *nmt81*::*gfp-atb2*$^+$ strain rescued by expression of Asp1^{H397A}. (A) Quantification of spindle phenotypes (gray and black bars show broken and nonbroken spindles, respectively) for the indicated strains expressing *nmt81*::*gfp-atb2*$^+$ (*asp1*$^+$ strain, $n = 37$; *asp1*^{H397A} strain, $n = 31$; *asp1*^{D333A} strain, $n = 21$; *, $P < 0.05$; ***, $P < 0.001$ [as determined by χ^2 test]). (B) Example of collapsing (*) *asp1*$^+$ and *asp1*^{D333A} spindles in the *nmt81*::*gfp-atb2*$^+$ strain background. Time between images, 30 s. Bar, 2 μm. (C) Top, photomicrographs of *asp1*$^+$ and *asp1*^{H397A} short spindles. Bar, 2 μm. Bottom, relative signal intensity of spindle midzone in *asp1*$^+$ (57.5 ± 14.3) and *asp1*^{H397A} (81.6 ± 11.4) cells expressing *nmt81*::*gfp-atb2*$^+$. Quantification of the fluorescence signal was as described for Fig. 1B ($n = 9$/strain; ***, $P < 0.0005$ using two-sample *t* test).

spindles collapsed in 86% of *nmt81*::GFP-Atb2 *asp1*^{D333A} cells (Fig. 2A and B, right panel). Movie S3 in the supplemental material shows an example of a cell in which the thin spindle midzone collapsed, generating two spindle halves which reformed into a bipolar spindle. In some instances, these spindles collapsed again (see Movie S3). In general, broken spindles reformed and were able to undergo spindle elongation in spindle phase III (an example is shown in Movie S3). The *asp1*^{D333A} strain fitness was not reduced severely by the presence of *nmt81*::GFP-Atb2 (see Fig. S1B in the supplemental material).

Intriguingly, the collapsed spindle phenotype of the *nmt81*::GFP-Atb2 strain was not observed for the *asp1*^{H397A} *nmt81*::GFP-Atb2 strain (Fig. 2A). We thus compared the relative fluorescence signal intensities of the spindle midzones of *asp1*$^+$ and *asp1*^{H397A} spindles in the *nmt81*::GFP-Atb2 background. The relative fluorescence signal intensity of the spindle midzone was significantly increased for *asp1*^{H397A} spindles compared to *asp1*$^+$ spindles (Fig. 2C) (signal intensities of 81.6 ± 11.4 and 57.5 ± 14.3 for *asp1*^{H397A} and *asp1*$^+$, respectively). We conclude that Asp1-generated IPPs regulate spindle midzone stability: *asp1*^{D333A} cells, which have no Asp1 kinase activity, often show abnormally thin spindle midzones and a high number of collapsing spindles, while *asp1*^{H397A} cells have more stable spindle midzones than wild-type cells expressing *nmt81*::GFP-Atb2.

Spindle collapse occurs prior to chromosome segregation. In order to determine at which mitotic stage spindle collapse occurred, we used a strain where the segregation behavior of chromosome I sisters and the SPBs could be monitored. The collapsing spindles observed in *asp1*^{D333A} strains expressing either SV40::GFP-Atb2 or *nmt81*::GFP-Atb2 were spindles of maximally 5 μm in length. Metaphase spindles are usually shorter, but abnormally long metaphase spindles can occur due to altered force-generating mechanisms (reviewed in references 30 and 31). To analyze the segregation behavior of the SPBs and chromosome I sisters in *asp1*^{D333A} mitotic cells, we used the SPB component Sad1-mCherry and cen1-GFP (centromere I-linked GFP) (8, 32, 33). The presence of Sad1-mCherry cen1-GFP did not negatively affect growth of the *asp1*^{D333A} strain (see Fig. S2A in the supplemental material). However, live-cell imaging of cells undergoing mitosis revealed that in 9% of mitotic cells, the distance between the SPBs first increased and then drastically decreased, indicating spindle collapse (Fig. 3A and B). In the *asp1*^{D333A} cell shown in Fig. 3B and C, the distance between the SPBs increased to 4.8 μm, followed by spindle collapse and a reduced distance between the SPBs of just 1.7 μm. In all cases analyzed, the cen1-GFP signals had not been segregated to the SPBs prior to spindle collapse.

The subcellular localization of the highly conserved Aurora kinase Ark1 is an indicator of the mitotic stage (34). Ark1 localizes in close proximity to centromeres/kinetochores in early mitosis and relocalizes to the spindle at the onset of anaphase B (34, 35). We thus analyzed Ark1-GFP localization in strains expressing SPB-localized Sid4-mCherry (36) and either *asp1*$^+$ or *asp1*^{D333A} (growth of such strains is shown in Fig. S2B in the supplemental material). As has been described previously for wild-type (*asp1*$^+$) cells, upon entry into mitosis, a strong Ark1-GFP signal between the two separated SPBs is observed, demonstrating proximal centromere/kinetochore localization (Fig. 3D, left panel). Entry in anaphase B results in loss of Ark1-GFP at the centromere/kinetochore and relocalization to the spindle (Fig. 3D, left panel). A similar Ark1-GFP localization was seen for *asp1*^{D333A} cells in early mitosis (Fig. 3D, right panels). However, the Ark1-GFP centromere/kinetochore signal persisted approximately twice as long as

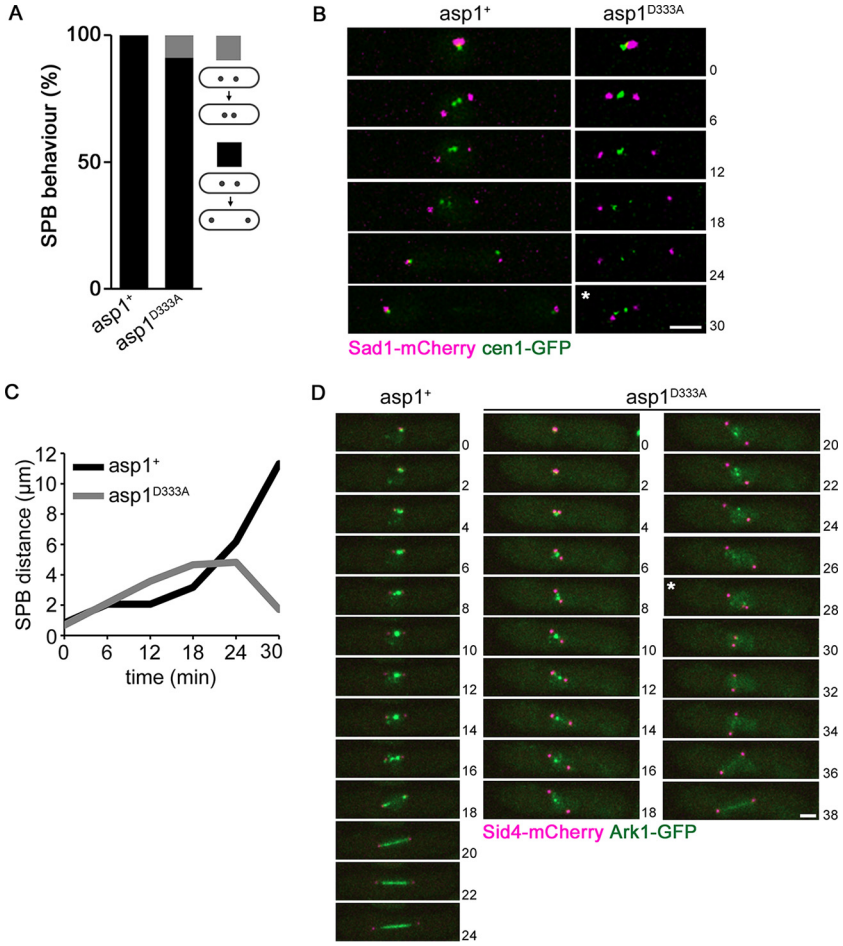

FIG 3 Spindle breakage occurs prior to sister chromatid segregation. (A) Quantification of SPB segregation phenotype determined for the indicated strains expressing cen1-gfp Sad1-mCherry (*asp1*$^{+}$ strain, $n = 31$; *asp1*^{D333A} strain, $n = 45$) (gray and black bars show collapsing and noncollapsing spindles, respectively). (B) Time-lapse images of mitotic *asp1*$^{+}$ and *asp1*^{D333A} cells expressing cen1-GFP Sad1-mCherry. Time between images, 6 min. Bar, 2 μm. *, time of spindle collapse. (C) Diagrammatic representation of the Sad1-mCherry images shown in panel B. (D) Localization of Ark1-GFP and Sid4-mCherry (= SPB position) in mitotic *asp1*$^{+}$ (left) und *asp1*^{D333A} (right) cells. Spindle collapse (*) was observed in the *asp1*^{D333A} cell. Time between images, 2 min. Bar, 2 μm.

that of wild-type cells and separated into several distinct spots that moved between the SPBs (Fig. 3D, right panels). These spots represent kinetochores not aligned in a bipolar manner. Upon spindle collapse (time point 28 min; the distance between SPBs changed from 4.5 to 1.1 μm), faint spot-like Ark1-GFP signals were observed, suggesting that spindle breakage occurs prior to anaphase B. Following spindle collapse, the spindle regenerated and the cell was able to finish mitosis, as indicated by the spindle localization of Ark1-GFP (Fig. 3D, right panels). Six of 33 analyzed *asp1*^{D333A} cells expressing Ark1-GFP Sid4-mCherry showed spindle collapse, and in these cases Ark1-GFP localization was comparable to that in the example shown. Interestingly in five of six cases with breaking spindles, the Ark1-GFP signal was greatly reduced just before spindle breakage. In addition, the Ark1-GFP signal intensity of *asp1*^{D333A} mitotic cells was reduced compared to that of *asp1*$^{+}$ cells. Measurement of the Ark1-GFP signal in prometaphase cells revealed a significant reduction in relative fluorescence signal intensity (*asp1*$^{+}$, 16.3 ± 3.4; *asp1*^{D333A}, 10.8 ± 3.3) (see Fig. S3A to C in the supplemental material).

Thus, our analysis of the cen1-GFP or Ark1-GFP subcellular localization in *asp1*^{D333A} cells shows that spindle collapse occurs prior to anaphase A completion.

Spindle phase I and III dynamics are regulated by Asp1 kinase activity. To determine if spindle formation (spindle phase I) and spindle elongation in anaphase B (phase III) were modulated by Asp1 kinase function, we determined the speed of SPB separation in the various *asp1* variant strains using Sad1-mCherry and cen1-GFP. For this analysis, we chose spindles that did not collapse. For spindle phase I, the measurements were done as follows: the first appearance of two Sad1-mCherry signals was defined as the starting point for the measurements, followed by determining the distance between the two separated SPB Sad1-mCherry signals for the successive 4 min (examples for *asp1*$^{+}$ and *asp1*^{D333A} cells are shown in Fig. 4A). At the end of the measurement, the average distance between SPBs of *asp1*$^{+}$ cells was 1.76 μm, while that between SPBs of *asp1*^{D333A} cells was 2.35 μm. SPBs in *asp1*$^{+}$ cells separated on average with a speed of 0.40 ± 0.06 μm/min, in accordance with previous measurements of spindle elongation at 20°C (8) (Fig. 4B). However, SPB separation in *asp1*^{D333A} cells was significantly faster; the average speed of separation was 0.50 ± 0.06 μm/min (Fig. 4B). Spindle phase I was not changed significantly in *asp1*^{H397A} cells compared to wild-type *asp1*$^{+}$ cells (Fig. 4B) (average speed of SPB separation in *asp1*^{H397A} cells, 0.43 ± 0.06 μm/min).

Similarly, spindle phase III, which encompasses spindle elon-

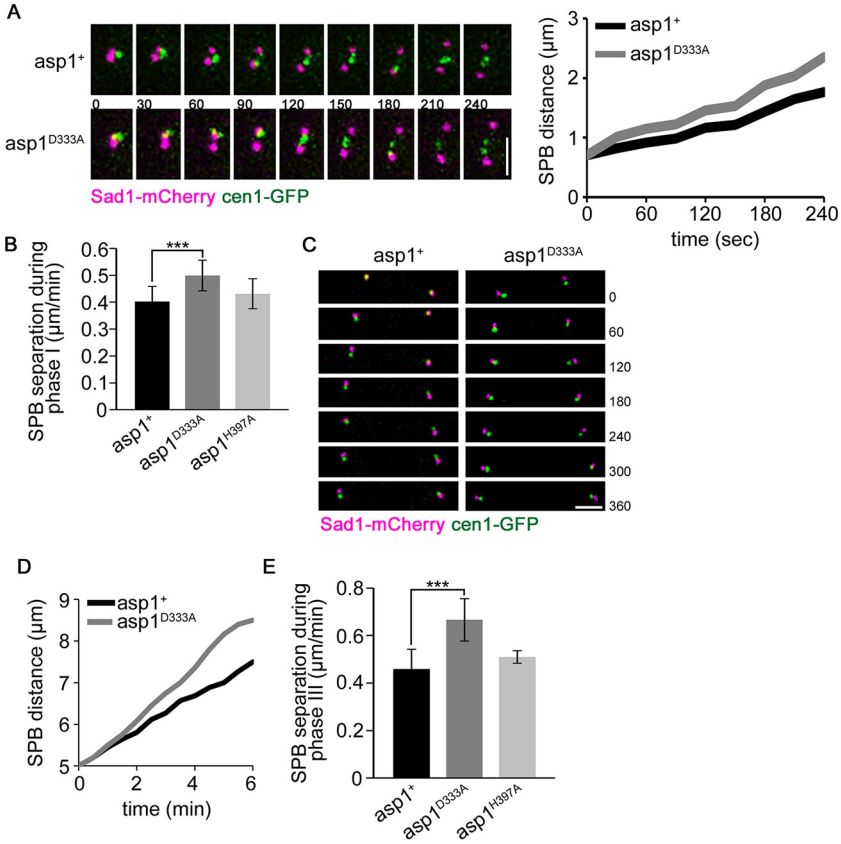

FIG 4 Spindle phases I and III are modulated by Asp1 kinase activity. (A) Left, live-cell imaging of Sad1-mCherry cen1-GFP-expressing wild-type (*asp1*$^{+}$) and *asp1*^{D333A} cells during prometaphase ($t = 0$ is first separation of SPBs). Time between images, 30 s. Bar, 2 μm. Right, distance between SPBs shown diagrammatically. (B) Diagrammatic representation of SPB separation speed during spindle phase I ($n = 20$/strain; ***, $P < 0.0005$ for the *asp1*^{D333A} strain compared to the *asp1*$^{+}$ strain [two-sample *t* test]). (C) Merged images of a wild-type (*asp1*$^{+}$) and an *asp1*^{D333A} anaphase B cell expressing Sad1-mCherry cen1-GFP. Time between images, 60 s. Bar, 2 μm. Cells with centromere signals with 5-μm distance ($t = 0$) were monitored by time-lapse microscopy to determine the speed of SPB separation. The time between images was 1 min, and cells were photographed for 6 min. At this time the average SPB distances were 7.5 and 8.5 μm for *asp1*$^{+}$ and *asp1*^{D333A} cells, respectively. (D) Diagrammatic representation of SPB separation of the cells shown in panel C. (E) Quantification of SPB separation during spindle phase III of the indicated strains: *asp1*$^{+}$ strain, 0.46 ± 0.08 μm/min; *asp1*^{D333A} strain, 0.67 ± 0.09 μm/min; *asp1*^{H397A} strain, 0.51 ± 0.03 μm/min ($n =$ 13/strain; ***, $P < 0.0005$ for the *asp1*^{D333A} strain compared to the *asp1*$^{+}$ strain [two-sample *t* test]). Start of measurement, separated cen1-GFP signal and a spindle length of 5 μm. Endpoint of measurement, 6 min after start of measurement.

gation by sliding apart of the polymerizing MT plus ends (9), was also modulated by IPPs. The speed of SPB separation in the various *asp1* strains was determined by analyzing mitotic cells with separated, SPB-proximal cen1-GFP signals. In the examples shown in Fig. 4C and D, the *asp1*$^{+}$ cell elongated the anaphase B spindle at a rate of 0.43 μm/min, while the *asp1*^{D333A} cell had a rate of 0.62 μm/min. In general we found that in *asp1*^{D333A} cells, spindle phase III elongation was significantly faster than in *asp1*$^{+}$ cells (Fig. 4E). In the majority of cases, the altered phase III dynamics observed for *asp1*^{D333A} phase III spindles did not result in spindle collapse. However, in some cells, phase III spindle collapse occurred (see Movie S4 in the supplemental material).

Analysis of SPB separation speed in *asp1*^{H397A} cells revealed that spindle phase III was comparable to that of wild-type cells (Fig. 4E).

Entry into anaphase A is prolonged significantly in *asp1*^{D333A} cells. To avoid aneuploidy, sister chromosomes need to establish bioriented attachments to spindle MTs before entry into anaphase A can proceed. Live-cell imaging of Sad1-mCherry cen1-GFP-expressing *asp1*$^{+}$ and *asp1*^{D333A} cells revealed that the mutant cell type took significantly longer to enter anaphase A (examples are shown in Fig. 5A and B). In the cases shown, the *asp1*$^{+}$ cell needed 18 min from the time of SPB separation to segregation of cen1-GFP signals to the SPBs, while the *asp1*^{D333A} cell needed 34 min for this process. Analysis of further *asp1*$^{+}$ and *asp1*^{D333A} mitotic cells revealed that the time needed for *asp1*^{D333A} cells to proceed to anaphase A was on average 54% longer than that for *asp1*$^{+}$ cells (Fig. 5C).

Prolonged delay before entry into anaphase leads to elongation of the *S. pombe* metaphase-like spindle. Indeed, we found that *asp1*^{D333A} anaphase A spindles were significantly longer than those of wild-type cells: *asp1*$^{+}$ cells segregated their cen1-GFP signals at an average spindle length of 3.5 μm, while *asp1*^{D333A} spindles were 4.7 μm at the onset of anaphase (Fig. 5D). Therefore, we tested whether the SAC was activated in the mutant cells, causing the observed delay.

SAC components Mph1 and Mad2 are required for the mitotic delay of *asp1*^{D333A} cells. Chromosome biorientation is a prerequisite for entry into anaphase A and is monitored by the SAC (reviewed in references 6 and 37). To determine if the mitotic

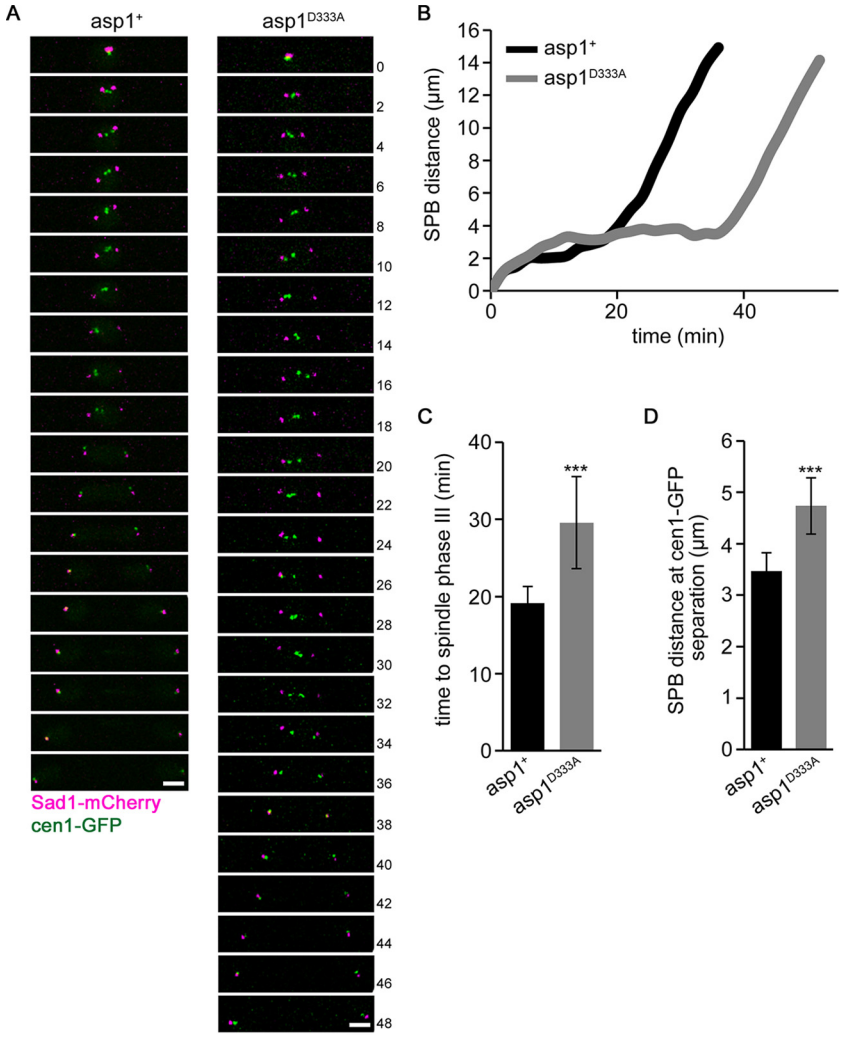

FIG 5 Asp1 kinase activity modulates entry into anaphase A. (A) Merged images of a mitotic cen1-GFP Sad1-mCherry wild-type (*asp1*$^{+}$) or *asp1*^{D333A} cell. Time between images, 2 min. Bars, 2 μm. (B) Diagrammatic representation of SPB distance versus time for the cells shown in panel A. (C) Diagrammatic representation of the time needed from prometaphase (separation of the SPBs) to anaphase A (segregation of cen1-GFP signals to SPB) in *asp1*$^{+}$ and *asp1*^{D333A} cells. (*asp1*$^{+}$ cells, 19.2 ± 2.1 min; *asp1*^{D333A} cells, 29.6 ± 5.9 min; $n = 19$/strain; ***, $P < 0.0005$ for *asp1*^{D333A} cells compared to *asp1*$^{+}$ cells [Welch test]). (D) Quantification of SPB distance at the time of cen1-GFP segregation in cen1-GFP Sad1-mCherry-expressing strains (*asp1*$^{+}$ strain, 3.5 ± 0.4 μm; *asp1*^{D333A} strain, 4.7 ± 0.5 μm; $n = 19$/strain; ***, $P < 0.0005$ for the *asp1*^{D333A} strain compared to the *asp1*$^{+}$ strain [two-sample *t* test]).

delay of *asp1*^{D333A} cells was caused by the SAC, we analyzed mitosis in SV40::GFP-Atb2^{+} *asp1*^{D333A} *mph1*Δ (deletion of the *mph1*$^{+}$ open reading frame [ORF]) cells (growth of strains is shown in Fig. S2C in the supplemental material). The *S. pombe* Mph1 protein is part of the SAC Mps1 kinase family and is at the top of the SAC signaling cascade (36, 38–42). *asp1*^{D333A} *mph1*Δ cells had a reduced fitness when grown on medium containing TBZ, implying that a functional Mph1 protein was necessary for the fitness of the *asp1*^{D333A} strain (Fig. 6A). Importantly, we found that the prolonged mitotic delay seen for *asp1*^{D333A} cells was abolished in *asp1*^{D333A} *mph1*Δ mitotic cells (examples are shown in Fig. 6B and C). Entry into spindle phase III (rapid spindle elongation) was on average twice as fast in *asp1*^{D333A} *mph1*Δ cells than in *asp1*^{D333A} cells (Fig. 6D).

Our analysis of the segregation behavior of cen1-GFP signals revealed that *asp1*^{D333A} cells showed chromosome missegregation. Eighteen percent of the *asp1*^{D333A} mitotic cells either displayed a lagging chromosome phenotype which was resolved during our measurements (Fig. 6E, light gray bars) or showed chromosome nondisjunction or chromosomes that were not moved to either SPB (Fig. 6E; these two phenotypes were scored together and are shown as dark gray box). Loss of Mph1 led to a further increase of the aberrant phenotype as determined for *asp1*^{D333A} *mph1*Δ cells (Fig. 6E).

Next we analyzed whether the prolonged mitotic delay of *asp1*^{D333A} cells was also dependent on a functional Mad2 protein (43, 44). *asp1*^{D333A} *mad2*Δ cells showed reduced growth on medium containing the MT-destabilizing drug TBZ (Fig. 7A). Importantly, the prolonged delay seen for *asp1*^{D333A} cells was abolished in *asp1*^{D333A} *mad2*Δ mitotic cells (representative examples are shown in Fig. 7B). Entry into spindle phase III (rapid spindle elongation) was significantly faster in *asp1*^{D333A} *mad2*Δ cells than in *asp1*^{D333A} cells (Fig. 7C).

We conclude that *asp1*^{D333A} cells, which cannot produce Asp1-

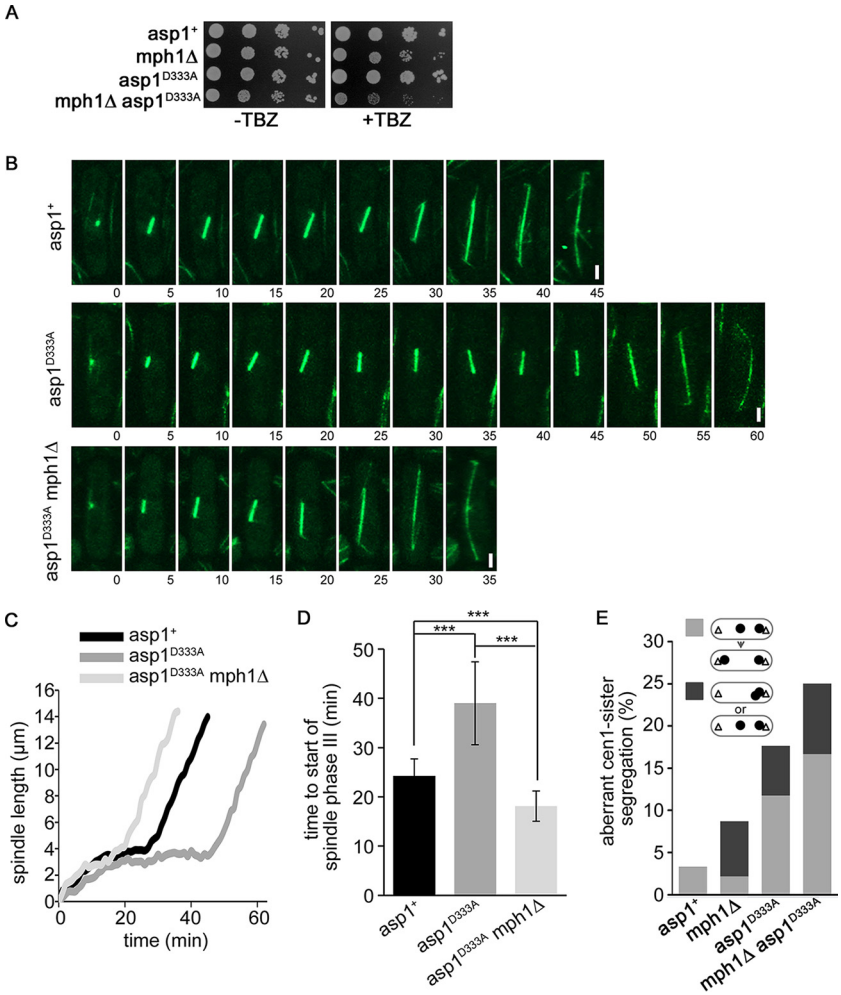

FIG 6 *asp1*^{D333A} cells require Mph1 for the prolonged delay into anaphase. (A) Serial dilution patch tests (10^4 to 10^1 cells) of the viability of the indicated strains on YE5S plates with (+TBZ) or without (−TBZ) 4 μg/ml TBZ. The plates were incubated for 4 days at 25°C. (B) Confocal live-cell images of the indicated strains expressing SV40::GFP-Atb2$^+$. Time between images, 5 min. Bars, 2 μm. (C) Diagrammatic illustration of mitotic spindle length over time for the cells shown in panel B. (D) Quantification of time required for transition from prometaphase to anaphase B due to spindle elongation of the indicated strains (*asp1*$^+$ strain, $n = 16$; *asp1*^{D333A} strain, $n = 16$; *asp1*^{D333A} *mph1*Δ strain, $n = 13$; ***, $P < 0.0005$ for the *asp1*^{D333A} *mph1*Δ [two-sample *t* test] and *asp1*^{D333A} [Welch test] strains compared to the *asp1*$^+$ strain and for the *asp1*^{D333A} *mph1*Δ [Welch test] strain compared to the *asp1*^{D333A} strain). (E) Phenotypes of aberrant cen1-GFP segregation behavior, i.e., lagging cen1-GFP signal that moved to the correct SPB during the time of measurement (light gray) or cen1-GFP signals both present at one SPB or a cen1-GFP signal that did not move to either SPB (dark gray) (*asp1*$^+$, $n = 62$; *mph1*Δ, $n = 46$; *asp1*^{D333A}, $n = 34$; *asp1*^{D333A} *mph1*Δ, $n = 36$).

generated IPPs, have defects in kinetochore-MT association and chromosome biorientation leading to chromosome missegregation. The SAC is active in such cells and can partially "rescue" the aberrant phenotype.

***asp1*^{H397A}-expressing cells proceed to anaphase A faster than wild-type cells.** Our finding that the absence of Asp1-generated IPPs led to a prolonged SAC-controlled delay of the entry into anaphase A raised the question of whether excess cellular IPPs might have the opposite effect. Therefore, we determined the length of spindle phases I and II in an *asp1*^{H397A} strain expressing SV40::GFP-Atb2. *asp1*$^+$ wild-type cells took an average of 24.3 min before entry into phase III, while this time was reduced significantly to an average of 16.4 min in *asp1*^{H397A}-expressing cells (Fig. 8A). An example for each strain is shown in Fig. 8B to D. In this example, the times to spindle phase III were 28 and 20 min for *asp1*$^+$ and *asp1*^{H397A} cells, respectively. Measurement of the time required to enter anaphase A was also assessed in *asp1*$^+$ and *asp1*^{H397A} cells expressing Sad1-mCherry cen1-GFP. In general, we found that cells of these strains needed less time for entry into anaphase A than the SV40::GFP-Atb2-expressing strains, possibly because the presence of SV40::GFP-Atb2 influenced spindle formation and chromosome biorientation. Nevertheless, on average *asp1*^{H397A} cells showed a significantly earlier segregation of the cen1-GFP signals than *asp1*$^+$ cells (see Fig. S4 in the supplemental material).

We next determined whether the faster entry into anaphase A led to increased chromosome missegregation. This was not the case. Missegregation of cen1-GFP signals in *asp1*$^+$ Sad1-mCherry cen1-GFP or *asp1*^{H397A} Sad1-mCherry cen1-GFP cells was not observed (*asp1*$^+$, $n = 62$; *asp1*^{H397A}, $n = 58$). Furthermore, the absence of *mph1*$^+$ in these strains resulted in missegregation in 3 of 46 cells in the *asp1*$^+$ background and 1 of 44 cells in the *asp1*^{H397A} background. Thus, the observed reduction of the time required for anaphase A entry did not affect the fidelity of chromosome segregation.

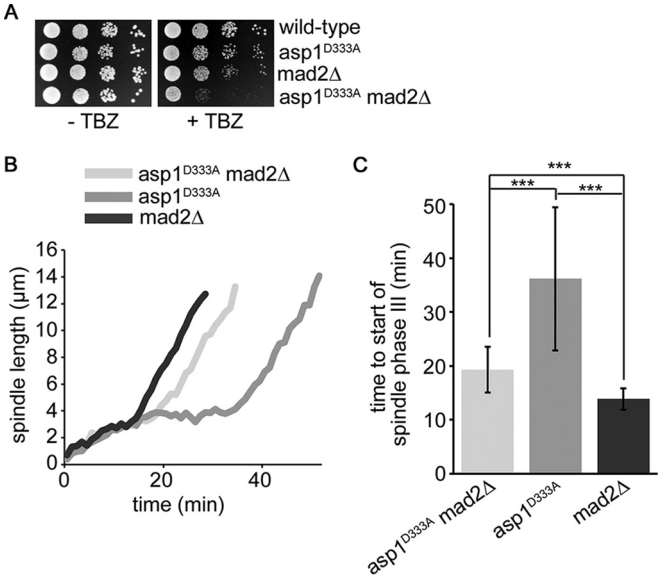

FIG 7 *asp1*^{D333A} cells require Mad2 for the prolonged delay into anaphase. (A) Serial dilution patch tests (10^4 to 10^1 cells) of the indicated strains grown on YE5S plates without and with 8 μg/ml TBZ. The plates were incubated for 5 days at 25°C. (B) Diagrammatic illustration of the spindle length over time. A representative example was chosen for each of the indicated strains expressing SV40::GFP-Atb2$^+$. (C) Quantification of the time required for the transition from prometaphase to anaphase B for the indicated strains (*asp1*^{D333A} *mad2*Δ strain, 19.3 ± 4.3 min; *asp1*^{D333A} strain, 36.2 ± 13.3 min; *mad2*Δ strain, 13.9 ± 2.0 min; *n* for all strains = 20. ***, $P < 0.005$ (two-sample *t* test).

We next determined the chromosome transmission fidelity of the nonessential Ch16 minichromosome (45) in cells that generated more IPPs than wild-type cells. The 550-kb Ch16 minichromosome can be maintained stably in a haploid *S. pombe* strain but is transmitted less faithfully than an endogenous chromosome, thus representing a sensitized system for the analysis of chromosome transmission fidelity (46). Loss of the minichromosome can be scored by the appearance of red sectors in a white colony (46). A Ch16-containing strain was transformed with a plasmid expressing the *asp1* variant *asp1*$^{1–364}$ via the thiamine-repressible promoter *nmt1*$^+$ (47). Asp1$^{1–364}$ (the Asp1 kinase domain) generates up to twice as much IPPs as full-length Asp1 *in vitro* (16). In addition, the plasmid-borne expression via the *nmt1*$^+$ promoter further ensured excess intracellular IPP production.

We found that approximately 1% of the colonies of the Ch16-containing strain transformed with a control vector were sectored, demonstrating loss of the minichromosome (Fig. 8E). This number was reduced 2-fold in transformants that expressed low levels of *asp1*$^{1–364}$ (i.e., basal expression of the *nmt1*$^+$ promoter in the presence of thiamine in the medium [+thia in Fig. 8E and F]). Furthermore, Ch16 minichromosome loss was further reduced when *asp1*$^{1–364}$ was expressed at a high level (i.e., derepression of the *nmt1*$^+$ promoter in the absence of thiamine in the medium [−thia in Fig. 8E and F]). In this case, loss of the minichromosome was reduced from 0.93% for the vector control transformants to 0.053% for cells expressing *asp1*$^{1–364}$ (Fig. 8E). This is a 17-fold reduction in Ch16 loss for *asp1*$^{1–364}$-expressing cells compared to cells transformed with the control vector.

Whether transmission fidelity of endogenous chromosomes was also increased in *asp1*^{H397A} cells compared to wild-type cells could not be determined conclusively due to the low number of segregation errors occurring for endogenous chromosomes. However, we found that in the presence of a small amount of TBZ (5 μg/ml), 76% of *mph1*Δ cells segregated the cen1-GFP signal correctly, while this number was increased to 83% in the *mph1*Δ *asp1*^{H397A} strain ($n = 51$ and 59, respectively).

Expression of Asp1$^{365–920}$ influences growth of strains with mutant motor proteins. To determine which process in spindle formation might be affected by Asp1 kinase function, we expressed the truncated Asp1 versions Asp1$^{1–364}$ and Asp1$^{365–920}$ (Asp1 kinase and phosphatase domains, respectively) via the *nmt1*$^+$ promoter on a plasmid in various strains with defective components of the mitotic spindle. We have shown previously that *in vitro* and presumably also *in vivo*, the presence of the Asp1 pyrophosphatase domain results in lower IPP output, while expression of the Asp1 kinase domain has the opposite effect (16). Interestingly, we found that the growth of *pkl1*Δ, *klp6*Δ, and *cut7-466*^{ts} mutant strains was affected in opposite manners by expression of Asp1$^{365–920}$. Klp6 is part of the heterodimer kinesin-8 Klp5/Klp6 which acts as an MT plus-end depolymerase, kinesin-14 Pkl1 is needed for anchoring of microtubule ends to the SPB, and the essential, spindle midzone-localized kinesin-5 Cut7 organizes bipolar MT interdigitation at the midzone (48–54). Klp5/6- and Pkl1-generated forces at the spindle act antagonistically to those of Cut7. Under the conditions tested, expression of Asp1$^{1–364}$ had little effect on the growth of the strains (Fig. 9), but expression of Asp1$^{365–920}$ rescued the temperature-sensitive nongrowth phenotype of the *cut7-466*^{ts} strain at 28°C (Fig. 9A) by increasing the number of surviving cells (Fig. 9B). In contrast, expression of Asp1$^{365–920}$ led to reduced growth of the *klp6*Δ strain and in particular of the *pkl1*Δ strain (Fig. 9C and D).

DISCUSSION

In this work we have discovered a mitotic function of the *S. pombe* member of the highly conserved Vip1 family. Asp1 kinase function is needed for the execution of all three stages of mitosis and controls bipolar spindle stability, chromosome biorientation, and the fidelity of chromosome transmission. This is the first report of a role for the high-energy IPP molecules in the regulation of fission yeast mitosis. Our previous analysis of Vip1 kinase interphase function in *S. pombe* and two distantly related filamentous fungi revealed that this enzyme family controls conserved biological processes (16). Thus, it is likely that our present findings will also be relevant for other mitotic systems. Indeed, a *Saccharomyces cerevisiae* synthetic genetic array analysis identified several negative interactions between *vip1*Δ (deletion of the Vip1-encoding ORF) and genes encoding mitotic components (55).

Spindle elongation dynamics are controlled by Asp1 kinase function. The bipolar spindle consists of kinetochore-MTs and interpolar MTs polymerized from both SPBs. Interpolar MTs from one SPB interdigitate with interpolar MTs from the other SPB at the spindle midzone to form a stable bipolar spindle cytoskeleton (reviewed in reference 25). Asp1 kinase function was required for all three spindle phases. Formation of the metaphase spindle (spindle phase I) requires the concerted action of MT-associated proteins and MT motor proteins such as the kinesin-5 class, which are responsible for sliding the antiparallel MTs apart. *asp1*^{D333A} cells showed a 46% faster separation of the duplicated SPBs than wild-type cells during the prometaphase stage. Furthermore, such cells often showed aberrant thin spindle midzones and

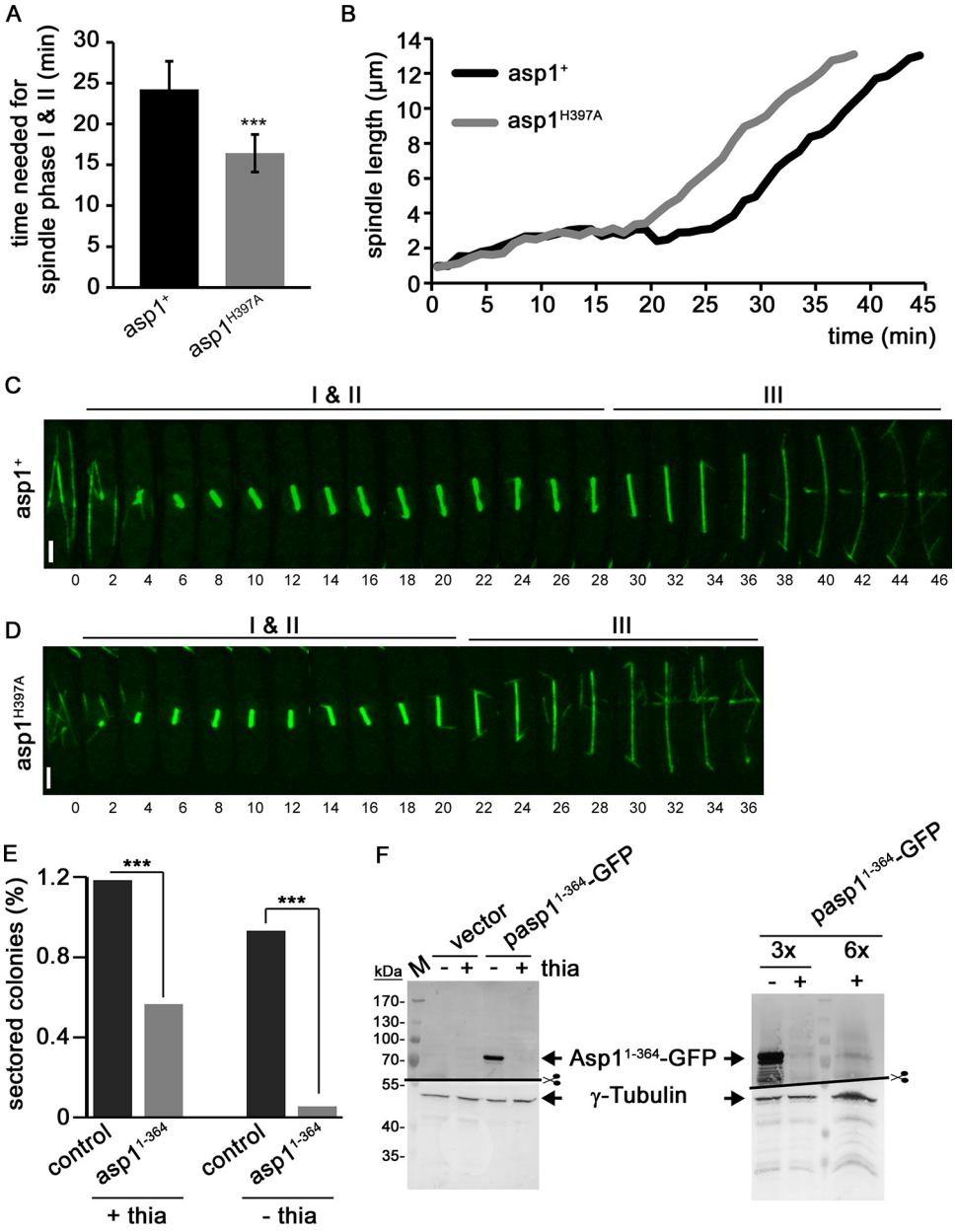

FIG 8 *asp1*^{H397A} cells reach spindle phase III faster than wild-type cells and show increased transmission fidelity of the Ch16 chromosome. (A) Diagrammatic representation of the times needed for spindle phases I and II as determined for *asp1*$^{+}$ and *asp1*^{H397A} cells expressing SV40::GFP-Atb2^{+} $n = 16$/strain; *asp1*$^{+}$ cells, 24.3 ± 3.4 min; *asp1*^{H397A} cells, 16.4 ± 2.3 min; ***, $P < 0.0005$ for *asp1*^{H397A} compared to *asp1*$^{+}$ cells [two-sample *t* test]). (B) Diagrammatic illustration of mitotic spindle length over time for the cells shown in panels C and D. (C and D) Confocal live-cell images of cells of the indicated strains expressing SV40::GFP-Atb2^{+}. Time between images, 2 min. Bars, 2 μm. (E) Diagrammatic representation of Ch16 loss (percent sectored colonies) in cells transformed with a control vector (control) or a plasmid expressing *asp1*$^{1–364}$ via the *nmt1*$^{+}$ promoter. +thia and −thia, presence or absence of thiamine, respectively, resulting in low or high Asp1$^{1–364}$ expression. For +thia: control, $n = 19{,}411$; Asp1$^{1–364}$, $n = 10{,}075$. For −thia: control, $n = 21{,}582$; Asp1$^{1–364}$, $n = 21{,}488$. (F) Western blot analysis of Asp1$^{1–364}$-GFP expressed in the presence or absence of thiamine. The blot on the right was overloaded (3 or 6 times the amount of protein used for the left blot) to visualize the Asp1$^{1–364}$ signal when thiamine was in the growth medium. γ-Tubulin protein was used as an internal control.

frequent spindle collapse. Remarkably, we made the observation that in *asp1*^{D333A} cells, spindle collapse was often followed by immediate chromosome segregation. A similar behavior has been described for the *cut7.24 klp6*Δ double mutant (56). Cut7 and Klp6 belong to the kinesin-5 and kinesin-8 families, respectively (48, 57), and are antagonistic spindle motors. The authors suggested that the "transient spindle shrinkage" might bring MT plus ends closer to kinetochores, thus facilitating attachment (56). This might also be the case in *asp1*^{D333A} cells, as such cells also have defects in chromosome-MT attachment.

How might Asp1-generated IPPs regulate spindle formation? IPPs are known to modulate cellular processes by two means: they regulate the function of a protein/protein complex either via reversible binding or by pyrophosphorylation (58, 59). Thus, direct

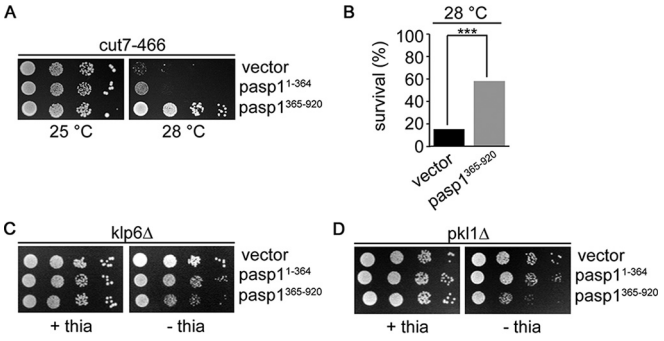

FIG 9 Plasmid-borne Asp1$^{365–920}$ expression rescues the temperature-sensitive nongrowth phenotype of the *cut7-466* strain. (A) Serial dilution patch tests (10^4 to 10^1 cells) of the *cut7-466* strain transformed with vector (control), *asp1*$^{1–364}$, or *asp1*$^{365–920}$ plasmid. Transformants were grown in thiamine-free medium under plasmid selective conditions at the indicated temperatures for 6 days. (B) Diagrammatic illustration of the survival of transformed *cut7-466* cells grown at the restrictive temperature of 28°C. Transformants were pregrown at 25°C under plasmid selective conditions that allowed expression of the *asp1* variants before plating cells at 28°C. Colony formation was assayed for 1,000 cells/transformant. ***, $P < 0.005$ (χ^2 test). (C and D) Serial dilution patch tests (10^4 to 10^1 cells) of the indicated strains transformed with the same plasmids as for panel A. The absence of thiamine results in derepression of the *nmt1*$^+$ promoter, which controls *asp1*$^{1–364}$ and *asp1*$^{365–920}$ expression. Plates were incubated at 25°C for 5 days.

binding of Asp1 to the IPP target protein might not be necessary. As Asp1 is a nuclear and cytoplasmic protein (reference 60 and our unpublished observations), it is feasible that IPPs generated in the nucleus modulate a component(s) of the mitotic spindle. Our previous analysis of the interphase microtubule cytoskeleton in *asp1*^{D333A} cells revealed that most microtubule parameters analyzed were altered, resulting in more dynamic microtubules (16). The EB1 family member Mal3, associated with spindle midzones, is not required for Asp1-mediated microtubule modulation (16, 61). Furthermore, localization of the midzone bundler Ase1/Prc1 was seemingly normal in *asp1*^{D333A} cells (references 62 and 63 and our unpublished observation). However, lowering intracellular IPP levels by plasmid-borne expression of Asp1$^{365–920}$ rescued the temperature-sensitive nongrowth phenotype of the *cut7-466* mutant strain, while negatively affecting growth of kinesin-14 *pkl1*Δ and kinesin-8 *klp6*Δ deletion strains. As Klp5/6 and Pkl1 act antagonistically to Cut7 and vice versa (53, 56), our results propose a function for IPPs in controlling the processes that balance the Cut7-generated outward force at the spindle.

Asp1-generated IPPs modulate chromosome transmission fidelity and control chromosome biorientation. Chromosome segregation errors in cells unable to produce Asp1-made IPPs were of the following two types: (i) chromosome nondisjunction, or the inability of chromosomes to be moved to either SPB, or (ii) chromosomes that lagged behind during anaphase. The first phenotype is a consequence of defective binding of spindle MTs to the kinetochore and can be detected by the SAC. Indeed, we found that chromosome biorientation was significantly delayed in *asp1*^{D333A} cells compared to wild-type cells. This delay was SAC dependent. Thus, Asp1-generated IPPs are required for biorientation of chromosomes.

Lagging chromosomes are not detected by the SAC. This behavior is caused by merotelic attachments where a single kinetochore is bound by MTs from either SPB. In mammalian cells the majority of aneuploidy events appear to arise by merotelic kinetochore-MT attachments (64). One of the consequences of merotelic attachments is the induction of the DNA damage response in human cell lines, leading to chromosomal aberrations in the progeny. This observation links aberrant mitosis with chromosome rearrangements (65).

Merotelic attachments are caused by hyperstabilized kinetochore-MT associations that need to be resolved by the Aurora B kinase-containing chromosome passenger complex present at the centromere/kinetochore (reviewed in references 66 and 67). Interestingly we found that the fluorescence intensity of the *S. pombe* Aurora kinetochore Ark1-GFP signal was reduced significantly in prometaphase *asp1*^{D333A} cells compared to wild-type cells. Abnormally low Ark1 concentrations might explain why erroneous kinetochore-MT attachments cannot be converted into correctly bioriented attachments, leading to an increased number of lagging chromosomes in *asp1*^{D333A} cells. Thus, Asp1-generated IPPs might be required for Ark1 kinetochore recruitment. How this might be achieved is at present unclear. However, it has been shown recently that spindle MTs via the conserved EB1 family play a role in the centromere targeting of human Aurora B (68). Thus, as IPPs modulate the MT cytoskeleton, the possibility exists that they affect Ark1 kinetochore targeting via this route.

Intriguingly, we found that cells that express the Asp1^{H397A} variant are able to enter anaphase A faster than wild-type cells, possibly because they were able to establish the correct chromosome biorientation faster. Furthermore, the transmission fidelity of the nonessential 550-kb Ch16 chromosome was increased in Asp1$^{1–364}$-expressing cells. Thus, higher-than-wild-type IPP levels increased the fidelity of Ch16 chromosome transmission beyond the frequency seen for the wild-type situation. Our data propose a direct correlation between intracellular IPP levels and genome integrity. How IPP levels modulate kinetochore-MT attachments is not clear. However, we previously found a direct correlation between IPP levels and the residence time of interphase MT plus ends at the cell cortex (16). Thus, IPPs might also control the residence time of spindle MT plus ends at the kinetochore interface, thus facilitating correct bipolar connections.

ACKNOWLEDGMENTS

We thank Jennifer Pöhlmann for help with Fig. S1 in the supplemental material and Robin Allshire, Kathleen Gould, Keith Gull, Iain Hagan, Silke Hauf, Alison Pidoux, Shelley Sazer, Takashi Toda, Mitsuhiro Yanagida, and the Yeast Genetic Resource Centre for the gifts of reagents used in this work. We are grateful to Shelley Sazer for critical input and careful reading of the manuscript and to the Center for Advanced Imaging (CAi) at the Heinrich-Heine-University, Düsseldorf, for help with microscopic analysis.

This research received no specific grant from any funding agency in the public, commercial, or not-for-profit sector.

FUNDING INFORMATION

This research received no specific grant from any funding agency in the public, commercial, or not-for-profit sector.

REFERENCES

1. **Baker DJ, Jeganathan KB, Cameron JD, Thompson M, Juneja S, Kopecka A, Kumar R, Jenkins RB, de Groen PC, Roche P, van Deursen JM.** 2004. BubR1 insufficiency causes early onset of aging-associated phenotypes and infertility in mice. Nat Genet **36**:744–749. http://dx.doi.org/10.1038/ng1382.
2. **Lott IT, Head E.** 2005. Alzheimer disease and Down syndrome: factors in

pathogenesis. Neurobiol Aging **26:**383–389. http://dx.doi.org/10.1016/j.neurobiolaging.2004.08.005.
3. **Harrison BD, Hashemi J, Bibi M, Pulver R, Bavli D, Nahmias Y, Wellington M, Sapiro G, Berman J.** 2014. A tetraploid intermediate precedes aneuploid formation in yeasts exposed to fluconazole. PLoS Biol **12:**e1001815. http://dx.doi.org/10.1371/journal.pbio.1001815.
4. **Santaguida S, Amon A.** 2015. Short- and long-term effects of chromosome mis-segregation and aneuploidy. Nat Rev Mol Cell Biol **16:**473–485. http://dx.doi.org/10.1038/nrm4025.
5. **Carmena M, Wheelock M, Funabiki H, Earnshaw WC.** 2012. The chromosomal passenger complex (CPC): from easy rider to the godfather of mitosis. Nat Rev Mol Cell Biol **13:**789–803. http://dx.doi.org/10.1038/nrm3474.
6. **Sacristan C, Kops GJ.** 2015. Joined at the hip: kinetochores, microtubules, and spindle assembly checkpoint signaling. Trends Cell Biol **25:**21–28. http://dx.doi.org/10.1016/j.tcb.2014.08.006.
7. **Akera T, Goto Y, Sato M, Yamamoto M, Watanabe Y.** 2015. Mad1 promotes chromosome congression by anchoring a kinesin motor to the kinetochore. Nat Cell Biol **17:**1124–1133. http://dx.doi.org/10.1038/ncb3219.
8. **Nabeshima K, Nakagawa T, Straight AF, Murray A, Chikashige Y, Yamashita YM, Hiraoka Y, Yanagida M.** 1998. Dynamics of centromeres during metaphase-anaphase transition in fission yeast: Dis1 is implicated in force balance in metaphase bipolar spindle. Mol Biol Cell **9:**3211–3225. http://dx.doi.org/10.1091/mbc.9.11.3211.
9. **Mallavarapu A, Sawin K, Mitchison T.** 1999. A switch in microtubule dynamics at the onset of anaphase B in the mitotic spindle of Schizosaccharomyces pombe. Curr Biol **9:**1423–1426. http://dx.doi.org/10.1016/S0960-9822(00)80090-1.
10. **Mulugu S, Bai W, Fridy PC, Bastidas RJ, Otto JC, Dollins DE, Haystead TA, Ribeiro AA, York JD.** 2007. A conserved family of enzymes that phosphorylate inositol hexakisphosphate. Science **316:**106–109. http://dx.doi.org/10.1126/science.1139099.
11. **Choi JH, Williams J, Cho J, Falck JR, Shears SB.** 2007. Purification, sequencing, and molecular identification of a mammalian PP-InsP5 kinase that is activated when cells are exposed to hyperosmotic stress. J Biol Chem **282:**30763–30775. http://dx.doi.org/10.1074/jbc.M704655200.
12. **Fridy PC, Otto JC, Dollins DE, York JD.** 2007. Cloning and characterization of two human VIP1-like inositol hexakisphosphate and diphosphoinositol pentakisphosphate kinases. J Biol Chem **282:**30754–30762. http://dx.doi.org/10.1074/jbc.M704656200.
13. **Gokhale NA, Zaremba A, Shears SB.** 2011. Receptor-dependent compartmentalization of PPIP5K1, a kinase with a cryptic polyphosphoinositide binding domain. Biochem J **434:**415–426. http://dx.doi.org/10.1042/BJ20101437.
14. **Lin H, Fridy PC, Ribeiro AA, Choi JH, Barma DK, Vogel G, Falck JR, Shears SB, York JD, Mayr GW.** 2009. Structural analysis and detection of biological inositol pyrophosphates reveal that the family of VIP/diphosphoinositol pentakisphosphate kinases are 1/3-kinases. J Biol Chem **284:**1863–1872. http://dx.doi.org/10.1074/jbc.M805686200.
15. **Wang H, Falck JR, Hall TM, Shears SB.** 2011. Structural basis for an inositol pyrophosphate kinase surmounting phosphate crowding. Nat Chem Biol **8:**111–116. http://dx.doi.org/10.1038/nchembio.733.
16. **Pöhlmann J, Risse C, Seidel C, Pohlmann T, Jakopec V, Walla E, Ramrath P, Takeshita N, Baumann S, Feldbrugge M, Fischer R, Fleig U.** 2014. The Vip1 inositol polyphosphate kinase family regulates polarized growth and modulates the microtubule cytoskeleton in fungi. PLoS Genet **10:**e1004586. http://dx.doi.org/10.1371/journal.pgen.1004586.
17. **Wang H, Nair VS, Holland AA, Capolicchio S, Jessen HJ, Johnson MK, Shears SB.** 2015. Asp1 from Schizosaccharomyces pombe binds a [2Fe-2S](2+) cluster which inhibits inositol pyrophosphate 1-phosphatase activity. Biochemistry **54:**6462–6474. http://dx.doi.org/10.1021/acs.biochem.5b00532.
18. **Pulloor NK, Nair S, Kostic AD, Bist P, Weaver JD, Riley AM, Tyagi R, Uchil PD, York JD, Snyder SH, Garcia-Sastre A, Potter BV, Lin R, Shears SB, Xavier RJ, Krishnan MN.** 2014. Human genome-wide RNAi screen identifies an essential role for inositol pyrophosphates in type-I interferon response. PLoS Pathog **10:**e1003981. http://dx.doi.org/10.1371/journal.ppat.1003981.
19. **Laha D, Johnen P, Azevedo C, Dynowski M, Weiss M, Capolicchio S, Mao H, Iven T, Steenbergen M, Freyer M, Gaugler P, de Campos MK, Zheng N, Feussner I, Jessen HJ, Van Wees SC, Saiardi A, Schaaf G.** 2015. VIH2 regulates the synthesis of inositol pyrophosphate InsP8 and jasmonate-dependent defenses in Arabidopsis. Plant Cell **27:**1082–1097. http://dx.doi.org/10.1105/tpc.114.135160.
20. **Feoktistova A, McCollum D, Ohi R, Gould KL.** 1999. Identification and characterization of Schizosaccharomyces pombe asp1(+), a gene that interacts with mutations in the Arp2/3 complex and actin. Genetics **152:**895–908.
21. **Pöhlmann J, Fleig U.** 2010. Asp1, a conserved 1/3 inositol polyphosphate kinase, regulates the dimorphic switch in Schizosaccharomyces pombe. Mol Cell Biol **30:**4535–4547. http://dx.doi.org/10.1128/MCB.00472-10.
22. **Moreno S, Klar A, Nurse P.** 1991. Molecular genetic analysis of fission yeast Schizosaccharomyces pombe. Methods Enzymol **194:**795–823. http://dx.doi.org/10.1016/0076-6879(91)94059-L.
23. **Tran PT, Paoletti A, Chang F.** 2004. Imaging green fluorescent protein fusions in living fission yeast cells. Methods **33:**220–225. http://dx.doi.org/10.1016/j.ymeth.2003.11.017.
24. **Bratman SV, Chang F.** 2007. Stabilization of overlapping microtubules by fission yeast CLASP. Dev Cell **13:**812–827. http://dx.doi.org/10.1016/j.devcel.2007.10.015.
25. **Winey M, Bloom K.** 2012. Mitotic spindle form and function. Genetics **190:**1197–1224. http://dx.doi.org/10.1534/genetics.111.128710.
26. **Snaith HA, Anders A, Samejima I, Sawin KE.** 2010. New and old reagents for fluorescent protein tagging of microtubules in fission yeast; experimental and critical evaluation. Methods Cell Biol **97:**147–172. http://dx.doi.org/10.1016/S0091-679X(10)97009-X.
27. **Kerres A, Jakopec V, Fleig U.** 2007. The conserved Spc7 protein is required for spindle integrity and links kinetochore complexes in fission yeast. Mol Biol Cell **18:**2441–2454. http://dx.doi.org/10.1091/mbc.E06-08-0738.
28. **Garcia MA, Vardy L, Koonrugsa N, Toda T.** 2001. Fission yeast ch-TOG/XMAP215 homologue Alp14 connects mitotic spindles with the kinetochore and is a component of the Mad2-dependent spindle checkpoint. EMBO J **20:**3389–3401. http://dx.doi.org/10.1093/emboj/20.13.3389.
29. **Jakopec V, Topolski B, Fleig U.** 2012. Sos7, an essential component of the conserved S. pombe Ndc80-MIND-Spc7 complex, identifies a new family of fungal kinetochore proteins. Mol Cell Biol **32:**3308–3312. http://dx.doi.org/10.1128/MCB.00212-12.
30. **Goshima G, Scholey JM.** 2010. Control of mitotic spindle length. Annu Rev Cell Dev Biol **26:**21–57. http://dx.doi.org/10.1146/annurev-cellbio-100109-104006.
31. **Costa J, Fu C, Khare VM, Tran PT.** 2014. csi2p modulates microtubule dynamics and organizes the bipolar spindle for chromosome segregation. Mol Biol Cell **25:**3900–3908. http://dx.doi.org/10.1091/mbc.E14-09-1370.
32. **Hagan I, Yanagida M.** 1995. The product of the spindle formation gene sad1+ associates with the fission yeast spindle pole body and is essential for viability. J Cell Biol **129:**1033–1047. http://dx.doi.org/10.1083/jcb.129.4.1033.
33. **Nakazawa N, Nakamura T, Kokubu A, Ebe M, Nagao K, Yanagida M.** 2008. Dissection of the essential steps for condensin accumulation at kinetochores and rDNAs during fission yeast mitosis. J Cell Biol **180:**1115–1131. http://dx.doi.org/10.1083/jcb.200708170.
34. **Petersen J, Paris J, Willer M, Philippe M, Hagan IM.** 2001. The S. pombe aurora-related kinase Ark1 associates with mitotic structures in a stage dependent manner and is required for chromosome segregation. J Cell Sci **114:**4371–4384.
35. **Kawashima SA, Tsukahara T, Langegger M, Hauf S, Kitajima TS, Watanabe Y.** 2007. Shugoshin enables tension-generating attachment of kinetochores by loading Aurora to centromeres. Genes Dev **21:**420–435. http://dx.doi.org/10.1101/gad.1497307.
36. **Heinrich S, Windecker H, Hustedt N, Hauf S.** 2012. Mph1 kinetochore localization is crucial and upstream in the hierarchy of spindle assembly checkpoint protein recruitment to kinetochores. J Cell Sci **125:**4720–4727. http://dx.doi.org/10.1242/jcs.110387.
37. **Overlack K, Krenn V, Musacchio A.** 2014. When Mad met Bub. EMBO Rep **15:**326–328. http://dx.doi.org/10.1002/embr.201438574.
38. **Millband DN, Hardwick KG.** 2002. Fission yeast Mad3p is required for Mad2p to inhibit the anaphase-promoting complex and localizes to kinetochores in a Bub1p-, Bub3p-, and Mph1p-dependent manner. Mol Cell Biol **22:**2728–2742. http://dx.doi.org/10.1128/MCB.22.8.2728-2742.2002.
39. **Windecker H, Langegger M, Heinrich S, Hauf S.** 2009. Bub1 and Bub3 promote the conversion from monopolar to bipolar chromosome attachment independently of shugoshin. EMBO Rep **10:**1022–1028. http://dx.doi.org/10.1038/embor.2009.183.
40. **Ito D, Saito Y, Matsumoto T.** 2012. Centromere-tethered Mps1 pombe

homolog (Mph1) kinase is a sufficient marker for recruitment of the spindle checkpoint protein Bub1, but not Mad1. Proc Natl Acad Sci U S A **109:**209–214. http://dx.doi.org/10.1073/pnas.1114647109.
41. **Yamagishi Y, Yang CH, Tanno Y, Watanabe Y.** 2012. MPS1/Mph1 phosphorylates the kinetochore protein KNL1/Spc7 to recruit SAC components. Nat Cell Biol **14:**746–752. http://dx.doi.org/10.1038/ncb2515.
42. **Lara-Gonzalez P, Westhorpe FG, Taylor SS.** 2012. The spindle assembly checkpoint. Curr Biol **22:**R966–980. http://dx.doi.org/10.1016/j.cub.2012.10.006.
43. **Saitoh S, Ishii K, Kobayashi Y, Takahashi K.** 2005. Spindle checkpoint signaling requires the mis6 kinetochore subcomplex, which interacts with mad2 and mitotic spindles. Mol Biol Cell **16:**3666–3677. http://dx.doi.org/10.1091/mbc.E05-01-0014.
44. **Heinrich S, Geissen EM, Kamenz J, Trautmann S, Widmer C, Drewe P, Knop M, Radde N, Hasenauer J, Hauf S.** 2013. Determinants of robustness in spindle assembly checkpoint signalling. Nat Cell Biol **15:**1328–1339. http://dx.doi.org/10.1038/ncb2864.
45. **Niwa O, Matsumoto T, Yanagida M.** 1986. Construction of a mini-chromosome by deletion and itsmitotic and meiotic behaviour in fission yeast. Mol Gen Genet **203:**397–405. http://dx.doi.org/10.1007/BF00422063.
46. **Fleig U, Sen-Gupta M, Hegemann JH.** 1996. Fission yeast mal2+ is required for chromosome segregation. Mol Cell Biol **16:**6169–6177. http://dx.doi.org/10.1128/MCB.16.11.6169.
47. **Maundrell K.** 1993. Thiamine-repressible expression vectors pREP and pRIP for fission yeast. Gene **123:**127–130. http://dx.doi.org/10.1016/0378-1119(93)90551-D.
48. **Hagan I, Yanagida M.** 1992. Kinesin-related cut7 protein associates with mitotic and meiotic spindles in fission yeast. Nature **356:**74–76. http://dx.doi.org/10.1038/356074a0.
49. **Garcia MA, Koonrugsa N, Toda T.** 2002. Spindle-kinetochore attachment requires the combined action of Kin I-like Klp5/6 and Alp14/Dis1-MAPs in fission yeast. EMBO J **21:**6015–6024. http://dx.doi.org/10.1093/emboj/cdf611.
50. **Garcia MA, Koonrugsa N, Toda T.** 2002. Two kinesin-like Kin I family proteins in fission yeast regulate the establishment of metaphase and the onset of anaphase A. Curr Biol **12:**610–621. http://dx.doi.org/10.1016/S0960-9822(02)00761-3.
51. **Erent M, Drummond DR, Cross RA.** 2012. S. pombe kinesins-8 promote both nucleation and catastrophe of microtubules. PLoS One **7:**e30738. http://dx.doi.org/10.1371/journal.pone.0030738.
52. **Grissom PM, Fiedler T, Grishchuk EL, Nicastro D, West RR, McIntosh JR.** 2009. Kinesin-8 from fission yeast: a heterodimeric, plus-end-directed motor that can couple microtubule depolymerization to cargo movement. Mol Biol Cell **20:**963–972.
53. **Yukawa M, Ikebe C, Toda T.** 2015. The Msd1-Wdr8-Pkl1 complex anchors microtubule minus ends to fission yeast spindle pole bodies. J Cell Biol **209:**549–562. http://dx.doi.org/10.1083/jcb.201412111.
54. **Syrovatkina V, Tran PT.** 2015. Loss of kinesin-14 results in aneuploidy via kinesin-5-dependent microtubule protrusions leading to chromosome cut. Nat Commun **6:**7322. http://dx.doi.org/10.1038/ncomms8322.
55. **Daniel JA, Keyes BE, Ng YP, Freeman CO, Burke DJ.** 2006. Diverse functions of spindle assembly checkpoint genes in Saccharomyces cerevisiae. Genetics **172:**53–65.
56. **Syrovatkina V, Fu C, Tran PT.** 2013. Antagonistic spindle motors and MAPs regulate metaphase spindle length and chromosome segregation. Curr Biol **23:**2423–2429. http://dx.doi.org/10.1016/j.cub.2013.10.023.
57. **West RR, Malmstrom T, McIntosh JR.** 2002. Kinesins klp5(+) and klp6(+) are required for normal chromosome movement in mitosis. J Cell Sci **115:**931–940.
58. **Lee YS, Mulugu S, York JD, O'Shea EK.** 2007. Regulation of a cyclin-CDK-CDK inhibitor complex by inositol pyrophosphates. Science **316:**109–112. http://dx.doi.org/10.1126/science.1139080.
59. **Saiardi A, Bhandari R, Resnick AC, Snowman AM, Snyder SH.** 2004. Phosphorylation of proteins by inositol pyrophosphates. Science **306:**2101–2105. http://dx.doi.org/10.1126/science.1103344.
60. **Matsuyama A, Arai R, Yashiroda Y, Shirai A, Kamata A, Sekido S, Kobayashi Y, Hashimoto A, Hamamoto M, Hiraoka Y, Horinouchi S, Yoshida M.** 2006. ORFeome cloning and global analysis of protein localization in the fission yeast Schizosaccharomyces pombe. Nat Biotechnol **24:**841–847. http://dx.doi.org/10.1038/nbt1222.
61. **Beinhauer JD, Hagan IM, Hegemann JH, Fleig U.** 1997. Mal3, the fission yeast homologue of the human APC-interacting protein EB-1 is required for microtubule integrity and the maintenance of cell form. J Cell Biol **139:**717–728. http://dx.doi.org/10.1083/jcb.139.3.717.
62. **Loiodice I, Staub J, Setty TG, Nguyen NP, Paoletti A, Tran PT.** 2005. Ase1p organizes antiparallel microtubule arrays during interphase and mitosis in fission yeast. Mol Biol Cell **16:**1756–1768. http://dx.doi.org/10.1091/mbc.E04-10-0899.
63. **Yamashita A, Sato M, Fujita A, Yamamoto M, Toda T.** 2005. The roles of fission yeast ase1 in mitotic cell division, meiotic nuclear oscillation, and cytokinesis checkpoint signaling. Mol Biol Cell **16:**1378–1395. http://dx.doi.org/10.1091/mbc.E04-10-0859.
64. **Cimini D, Howell B, Maddox P, Khodjakov A, Degrassi F, Salmon ED.** 2001. Merotelic kinetochore orientation is a major mechanism of aneuploidy in mitotic mammalian tissue cells. J Cell Biol **153:**517–527. http://dx.doi.org/10.1083/jcb.153.3.517.
65. **Janssen A, van der Burg M, Szuhai K, Kops GJ, Medema RH.** 2011. Chromosome segregation errors as a cause of DNA damage and structural chromosome aberrations. Science **333:**1895–1898. http://dx.doi.org/10.1126/science.1210214.
66. **Ruchaud S, Carmena M, Earnshaw WC.** 2007. Chromosomal passengers: conducting cell division. Nat Rev Mol Cell Biol **8:**798–812. http://dx.doi.org/10.1038/nrm2257.
67. **Bakhoum SF, Thompson SL, Manning AL, Compton DA.** 2009. Genome stability is ensured by temporal control of kinetochore-microtubule dynamics. Nat Cell Biol **11:**27–35. http://dx.doi.org/10.1038/ncb1809.
68. **Banerjee B, Kestner CA, Stukenberg PT.** 2014. EB1 enables spindle microtubules to regulate centromeric recruitment of Aurora B. J Cell Biol **204:**947–963. http://dx.doi.org/10.1083/jcb.201307119.